Contemporary Mathematics
Volume 141, 1993

On the Significance of Unsteady Effects in the Aerodynamic Performance of Flying Animals

G.R. SPEDDING

ABSTRACT. The relative importance of unsteady effects in flapping animal flight is a frequent topic of discussion, some 35 years following the first classic studies. Here, we identify contributions both from the kinematics of the lifting surface and from oscillatory motions arising spontaneously in the viscous boundary layer. There exists convincing experimental evidence that the much-used two-dimensional, steady-state, blade-element analysis is inadequate even for relatively modest values of the frequency parameter, $k \equiv \omega c/2U \approx 0.4$. This result is actually quite consistent with recent theoretical analyses where unsteady and three-dimensional wake corrections have been computed for $k \ll 1$, $\Omega \equiv kAR = O(1)$ for an unsteady lifting line with centerline curvature, and for $k = O(1)$ for rigid unswept wings. Selected results from such (inviscid) models are discussed to illustrate how the first-order unsteady and three-dimensional corrections can be computed and shown to be of importance over much of the k range applicable to forward flapping animal flight. Problems involving flow separation, transition to turbulence, and numerical estimation of the form drag of irregularly shaped objects are hard, important, and remain open for realistic applications to animal flight at moderate Reynolds numbers. Some practical examples are given. It is argued that the usual dichotomy of the unsteady versus steady-state aerodynamics debate be replaced by a more quantitative approach where the *magnitude* of such effects is estimated. Certain outstanding problems and promising research topics and technologies are identified, many of which are concerned with a satisfactory accounting of viscous forces in the flow field.

1. Introduction and definitions

The motivation behind this essay stems from research that went into the writing of a review article (Ref. 1), when it became apparent that there exists a considerable gap between the biological and the aerodynamics/applied-mathematics literatures when discussing the rôle of unsteady effects in animal flight. Recent

1991 *Mathematics Subject Classification.* Primary 76.
This paper is in final form and no version of it has been submitted for publication elsewhere.

0271-4132/93 $1.00 + $.25 per page

progress in modeling and quantitative understanding of unsteady flows appears to have been largely ignored by the biology community, partly because these same models may be framed in terms that are either not understandable, or are of arguable practical significance to the scientist who must deal with phenomena seemingly far removed from the convenient and elegant simplifications of the theoretician. Here we attempt to identify some of these gaps, and propose solutions to fill others.

The discussion will be centered on the question: "What is the *significance* of *unsteady* effects in the *aerodynamic performance* of *flying animals*?" Each of the italicized terms must be defined so as to restrict the discussion to less than encyclopedic size. The aerodynamic performance considerations will be confined to knowledge of the instantaneous and integrated normal forces on the lifting surfaces during a single wing-stroke period T. Only flapping flight in still air will be considered. In the absence of any separate thrust generator, and without the benefit of continuous rotating machinery, the wings must therefore oscillate to provide both lift and thrust, and as a consequence there will *always* be some time-varying component of the normal forces. The significance of these effects depends somewhat on the original purpose of the investigator. Since it thus becomes a moving target, we can replace it with the *magnitude*, and leave the general discussion of the modeling enterprise to other forums (Ref. 1).

In an unsteady flow, the fluid velocity $\vec{u}$ is a function of time somewhere in the spatial domain of interest,

$$\vec{u} = \vec{u}(\vec{x}, t).$$

Given the restrictions outlined above, in an incompressible fluid, one is interested primarily in time-varying velocities (and pressures) at the lifting surface $\vec{s}$,

$$\vec{u}_s = \vec{u}_s(\vec{s}, t).$$

It is not necessary that $\vec{s} = \vec{s}(t)$, and the effects of separation, vortex shedding, and transition to turbulence may dramatically alter the fluid flow, without any motion of the body itself. To simplify somewhat, one can distinguish two sources of unsteadiness over a lifting surface:

1. Unsteady motion in the viscous boundary layer of an object that is immersed in a steady free stream. The oscillation frequency is a dependent function of the Reynolds number, Re. Boundary-layer separation, and possibly reattachment over bluff bodies, is very sensitive to changes in U, l, and in the geometry of the surface.
2. Terms arising from the existence of a third parameter, independent of Re, such as a frequency of oscillation of the body, ω (*cf.* Ref. 2, p. 211).

The analysis for the former viscous problem is rather complex, and we shall return to it later. The latter problem has been investigated in inviscid flows for a broad range of dimensionless frequency parameters, which can be defined based

on the mean half chord, or on the semispan as

$$k \equiv \frac{\omega \bar{c}}{2U}, \tag{1}$$

and

$$\Omega \equiv \frac{\omega b}{U}. \tag{2}$$

Note that $AR \equiv \frac{2b}{\bar{c}}$, so $\Omega = kAR$. Dynamical similarity of any two flows now requires that both Re and k (and Ω, when appropriate) be the same. The parameter k is a measure of the ratio of the period of oscillation to the mean flow transit time, and Ω can be thought of as a measure of the ratio of crosstream to streamwise vorticity in a three-dimensional flow. We shall use them as a measure of the unsteadiness in item (2) above.

2. Blade-element analysis

2.1 Method.

The standard example of this approach, which necessarily assumes steady, two-dimensional flow, is that of Weis-Fogh and Jensen (Refs. 3–5) on the desert locust, *Schistocerca gregaria*. They measured the lift and drag coefficients of isolated wings in the wall boundary-layer of a wind tunnel, and calculated the local section (Fig. 1) lift and drag forces from equations of the form,

$$\begin{aligned} L'(r,t) &= \frac{1}{2}\rho \vec{u}^2 c_l S', \\ D'(r,t) &= \frac{1}{2}\rho \vec{u}^2 c_d S'. \end{aligned} \tag{3}$$

Then the time-averaged lift force can be written as

$$\overline{L} = \frac{1}{T}\int_0^T \int_0^R [L'_v(r,t) + D'_v(r,t)]\, dr\, dt, \tag{4}$$

where L'_v and D'_v are the vertical components of the lift and drag. When the locusts were measured to be supporting their weight, the calculated lift and drag forces agreed with those measured to within 7%. Since c_l and c_d were steady-state measurements, the implication was that steady-state aerodynamics were sufficient to account for the aerodynamic performance, contrary to prevailing opinions at the time (Ref. 3).

Further simplifications of this argument are possible, so that if local wing incidence and geometry result in c_l and c_d being spanwise constant, and if w_i, the induced, downwash velocity, is similarly constant, then only expressions for the wing-beat kinematics and geometry remain inside the integrals of equation (4):

$$\begin{aligned} \int_0^T W\, dt = \rho \overline{C}_L \int_0^T \int_0^R \vec{u}^2(r,t) S'(r) \cos\psi\, dr\, dt \\ + \rho \overline{C}_D \int_0^T \int_0^R \vec{u}^2(r,t) S'(r) \sin\psi\, dr\, dt, \end{aligned} \tag{5}$$

where ψ is a simplified representation of the vector sum of the projected angles of incidence of the local wing section at r. In hovering flight, the projection geometry is simplified as a result of the absence of a mean flow, and Weis-Fogh (Ref. 6) outlined a number of simple wing shapes for which analytic solutions to equation (5) could be written. The technique has since been applied to the forward flight of birds, bats, and insects (e.g. Refs. 7–9) The logical argument then proceeds along similar lines: given the wing-beat kinematics, $\overline{C}_L$ and $\overline{C}_D$ are computed and compared with plausible steady-state values for such an airfoil section at the Reynolds number in question. Depending on whether these are exceeded, the initial steady-state hypothesis can be rejected, or supported. Note that this kind of inductive reasoning cannot confirm the sufficiency, or predominance, of steady-state mechanisms. It can only be used as grounds for rejecting such arguments.

2.2 Limitations.

Recently, Dudley and Ellington found that at *no* forward flight speed, from maximum to hovering, were the aerodynamics of the bumblebee consistent with the required time-averaged lift coefficients (Ref. 9). A quick calculation shows that $k = 0.15$ for the locust, and the lowest k for the bumblebee was 0.4 (the respective values of Ω are 1.64 and 2.65). It is therefore not particularly surprising that unsteady effects are more pronounced for the forward flight of the bumblebee. A comparison of the projected wingtip traces through the air for the two species (Figure 2) reveals certain interesting differences in trajectory shape and stroke plane angle that will not be reflected by a simple frequency parameter such as k. However, the most pronounced difference is in the number of chord lengths traveled by a wing section per wing beat, and the figure suggests that k could be a satisfactory measure of this (if this were the *only* difference, then the two traces would collapse on top of each other). Certain complications do arise though. For example, the large-amplitude fluctuations recorded in the instantaneous lift forces acting on a locust in level, unaccelerated flight (Ref. 10) are difficult to reconcile with the steady-state interpretation. Moreover, since the locust hindwing, which is responsible for 70% of the total lift (Ref. 5), has a mean chord length about twice that of the forewing, $k \approx 0.3$ for this lifting surface, approaching the bumblebee value. Should one now conclude that unsteady effects cannot be neglected here? Is there a numerical value of k where some cutoff point can be marked? It increasingly appears that the imposition of a binary steady/unsteady classification onto a continuous phenomenon (the magnitude of the unsteady forces) cannot do justice to the problem. Such an approach has its roots in historical necessity, but perhaps does not adequately reflect the recent progress in unsteady aerodynamical models. The following two sections explore some of these alternatives.

3. An unsteady three-dimensional lifting line with centerline curvature

Cheng and Murillo developed an asymptotic analysis of an inviscid, incompressible, potential flow about a high-aspect-ratio ($AR \equiv 2b/c_0 \gg 1$; c_0 is the centerline reference chord), planar lifting surface that oscillated at reduced frequencies $\Omega = O(1)$ (since $k = \Omega/AR, k \ll 1$) (Ref. 11). The theory is linear, so small disturbances from a planar wake and wing configuration are assumed. Chopra (Ref. 12) and Katz and Weihs (Ref. 13) have shown that corrections for large amplitude motion can be small, provided that k is small, and that transverse motions are of the same order as c_0. The results can thus tentatively be applied to the oscillatory propulsion of wings and tails of real animals, where the domain $\Omega = O(1)$ is very common. Karpouzian et al. carried out an extensive performance analysis of this model, and the propulsive efficiency,

$$\eta \equiv \frac{U\langle T\rangle}{\langle P\rangle}, \tag{6}$$

where $\langle T\rangle$ and $\langle P\rangle$ are the time-averaged thrust and power, was reported for a range of geometric and kinematic parameters, for *realistic* values of the thrust coefficient $\langle C_T\rangle$ – realistic in the sense that sufficient thrust must be generated to more than overcome the expected parasite drag on the lifting surface (Ref. 14). Comparisons of η and K (the average sweep) were made for fixed $\langle C_T\rangle$, by varying the local proportional feathering parameter (in the sense of Lighthill, Ref. 15; see Ref. 14 for details). Two families of lunate planforms, varying AR and K, are shown in Figure 3. Figure 4 shows $\eta(K)$ for three different values of $\langle C_T\rangle$. Note that η falls with increasing $\langle C_T\rangle$, and there appears to be an optimum sweep which increases with increasing $\langle C_T\rangle$. For $\langle C_T\rangle = 0.6$, the dashed line shows the leading-order terms only, equivalent to the two-dimensional quasi-steady strip theory. The three-dimensional and unsteady corrections are responsible for a significant reduction in η, $\approx 9\%$ at the optimum $K = 0.7$. This result is for $\Omega = 1.5$ ($k = 0.15$). The full three-dimensional, unsteady result does not show the asymptotically increasing η with K implied by the two-dimensional calculation.

The three-dimensional unsteady theory allows comparisons to be made of different planform geometries, and Figure 5 shows a comparison of the performance of the lunate shape (parabolic centerline) with a V-shape, for $\langle C_T\rangle = 0.6$ and $\Omega = 1.0$. The efficiencies for the lower solid curve are lower than for the equivalent case (again, the lower solid curve) in Figure 4, since Ω is lower. At high K, the V-shape appears more efficient, but this advantage disappears, both with decreasing K and when small changes in the major pitch-axis location and its transverse displacement are allowed. Note that there now appears to be an optimum K, and further increases in the heaving amplitude of the major pitch axis reduce this to zero. Such performance measurements enabled hydrodynamic arguments to be advanced for the apparent preference of the crescent-moon fin shape over the V-shape at moderate sweep angles, and for the large sweep angles

frequently found in V-shaped fins.

4. Other unsteady methods

Two further examples will serve to demonstrate how a more quantitative estimate of the magnitude of first-order unsteady terms in animal flight can be made.

4.1 A three-dimensional unsteady lifting line for planar wings and $k = O(1)$.

Phlips developed a three-dimensional unsteady lifting-line theory for planar, rigid, unswept wings of high AR. It is based on a simplified model of the vortex wake, divided into near- and far-wake regions (Ref. 16). Transverse vortices are shed at the extremes of the wing stroke, where they roll up, and they are represented by a single line-vortex. Streamwise vortices are shed at the trailing edge and they are assumed to remain in the path traced by the wings. In the far-wake, they collect into trailing vortex lines. This model simplifies the calculation of wake-induced velocities on the flapping wing, and the normal force on the wing was calculated assuming a linear $c_l(\alpha)$. These assumptions effectively restrict the analysis to moderate values of k. When the wing-beat amplitude ϕ exceeded approximately 60°, significant departures from the steady-state calculations were reported, particularly for $k > 1$. The effect of the induced velocity field in the unsteady calculation was to *increase* the value of the mean lift coefficient ($\approx$ 20% for $\phi = \pi/2$, $k = 2$), but the mean thrust coefficients were reduced slightly, so that the efficiency η fell with increasing k. In such a theory, spanwise flow along the wing and flow separation are ignored, but the clear implication is that unsteady terms cannot be neglected for $k > 1$.

4.2 Local circulation method.

The local circulation method and its application to dragonfly flight have been described by Azuma and co-workers (Ref. 17) (LCM I), and subsequently refined by Azuma and Watanabe (Ref. 18) (LCM II). It combines the approach of a blade-element analysis of wing sections with a more realistic and complete analysis of the modifying effects of the unsteady wake. The wing planform and initial circulation distribution is approximated by the superposition of a series of elliptical load distributions of diminishing size, each operating in the appropriate local shear flow, based on a thorough kinematic analysis of the animal in flight. The wake model consists of the trailing and transverse (in LCM II) vortices fixed by the path of the wingtip and trailing edge; an iterative procedure is applied for the wake corrections to the circulation distribution. Nonlinear, empirical $c_l(\alpha)$ curves were used to compute the forces and moments on the wings at each blade element. Since the computations are quite lengthy, the wake-attenuation coefficients were actually calculated only at $0.75R$.

The LCM I method was applied to the slow climbing flight of a dragonfly, for which k and Ω, as defined here, were approximately 1.6 and 16, respectively.

Both wings operated well away from the linear $c_l(\alpha)$ range for a substantial portion of the wing stroke. First-order unsteady effects were accounted for and shown to be significant improvements over actuator disk-based estimates of constant downwash over the span, but no other special high-lift mechanisms requiring large-scale separated flows were required to balance the forces in the analysis. The conclusions were similar for the LCM II study of the free flight of a dragonfly in a wind tunnel ($0.2 \leq k \leq 1.2$; $3.2 \leq \Omega \leq 12$). The comparison of LCM II with a standard blade-element calculation (constant w_i) at the highest flight speed, $U = 3.2$ m/sec, and consequently lowest k and Ω (= 0.2 and 3.2, respectively) revealed much smaller (around 20%) differences in the vertical forces than in the thrust (factors of 2–3), both for the instantaneous, and time-averaged values. Note that neither correction can be considered negligible.

5. Practical issues: laboratory examples

Thus far, a number of theoretical analyses have been shown to be capable of making quantitative predictions of the sign and magnitude of the unsteady terms for an oscillating lifting surface, at frequencies (but not necessarily amplitudes) close to those found in natural flight. Two examples from laboratory investigations of two-dimensional unsteady flows, where instantaneous force measurements were made simultaneously with flow visualization, will indicate the potential significance of unsteady forces, together with the strong influence of viscous effects in the form of large-scale separation bubbles.

5.1 Translational acceleration.

Gursal and Ho measured the instantaneous lift forces on a NACA 0012 aerofoil at a constant angle of attack ($\alpha = 20°$) in an unsteady free stream (Ref. 19). The instantaneous streamlines of Figure 6a show the growth and later removal of a separation bubble, based on the original streak photographs. The cycle begins at the start of the deceleration of the mean flow, which is sinusoidal with the form $U/U_\infty = 1 + R\cos\omega t$; in Figure 6, $R = 0.70$. The shear layer is already separated, but reattaches downstream. As the deceleration continues, up until $t/T = 0.5$, the bubble grows while remaining attached to the upper aerofoil surface. When the free stream begins to accelerate once again, the separation vortex is convected away downstream. Values of the instantaneous lift coefficient, $C_L(t) = L(t)/\frac{1}{2}\rho S U(t)^2$, (Fig. 6b) at the point of minimum free-stream velocity can reach 14. In interpreting these results, it should be noted that the magnitude of the lift force itself follows, in general, the amplitude of the free-stream velocity U, and is lowest when U is at its minimum. It is the lift *coefficient*, normalized by $U(t)^2$, that is high, far from its usual steady-state values at the same U. These high lift coefficients cannot be attributed to added mass effects since the peak C_L occurs when $dU/dt = 0$; moreover, the average acceleration is zero. Instead the high C_L must be a result of the strong pressure gradients normal to the wing owing to the vortex itself. Indeed, at this $Re = 5 \times 10^4$, 20° is beyond

the static stall angle, and in a steady mean flow, the surface pressures are *still* dominated by unsteady motions in the boundary layer.

5.2 Rotational acceleration.

The considerable modifying influence of viscous effects and separated flows can also be observed in the celebrated Weis-Fogh clap and fling mechanism (Refs. 6, 20–23) where flow separation occurs at the sharp leading edges of opening wing pairs at a wide range of Reynolds numbers (documented from 20 to 10^4). The isovorticity contours of Figure 7 (from data in Ref. 23) show that at $Re = 3 \times 10^3$ the distribution of vorticity can be quite complicated. In the early stages of motion the flow is always asymmetric, the outer edge of the vortex core can be rather disorganized (the core itself can be turbulent), and secondary vortices are generated at the lower wing surface and tips during the latter stages. The relative magnitude of some of these effects may be quite sensitive to changes in the wing opening time-history, but both quantitative flow visualization and simultaneous force measurements indicate that large time-averaged lift coefficients, $\langle C_L \rangle = 7 - 8$, can be achieved over a half-stroke (Fig. 8) (Ref. 23). The highest instantaneous lift forces are recorded toward the middle of the opening cycle, when the wing angular velocity is almost constant, implying that it is the vortex-induced lift that is responsible for the high C_L values. This separated flow has also been resolved in a direct numerical solution of the Navier-Stokes equations (Ref. 25) for the lower $Re = 30$.

6. Flow separation, transition to turbulence

Although one can make the case that many first-order unsteady effects may be adequately treated in certain models for oscillating animal wings at reasonable values of k and Ω, the same models cannot treat the separated flows such as those discussed in the previous section. Here, selected issues of separation and transitional flow in *steady* flows are surveyed.

6.1 Airfoil properties for $Re \approx 10^4$ to 10^6.

Lissaman has clearly noted how the performance of airfoils around the Reynolds number range of 10^4 to 10^6 may be dominated by the presence or absence of separation or by subsequent reattachment of the fluid over the lifting surface (Ref. 26). The presence of roughness, small fluctuations in the free-stream velocity or pressure gradients, the geometry of the lifting surface itself, and even the previous state of the boundary layer can have a significant effect on the airfoil performance. Cheng and Smith have analyzed the effect on separation of airfoil thickness and Re (Ref. 27). One aspect that can also have ramifications in the time-varying nature of the flow is illustrated in Figure 9, where considerable hysteresis is observed for $c_l(\alpha)$ of a thick and thin airfoil section at $Re = 10^5$. Over a range of α, which itself depends on both the geometry and Re, the lift is not single-valued. This can give rise to strong fluctuations in the lift as the flow oscillates between the various possible values. Lee and Cheng have iden-

tified bifurcations in the steady-state solutions of the boundary-layer equations for laminar flow over thin obstacles, suggesting that these could correspond to the lift hysteresis phenomenon (Ref. 30).

6.2 Transition.

Transition to turbulence may occur in the attached boundary layer, or more likely in the separated free-shear layer, which is less stable. Reattachment is greatly facilitated when the separated region is turbulent, a result of increased momentum transfer and entrainment of fluid from the free stream. Reattachment of laminar separation bubbles is not common below a critical value of Re, often quoted as $Re_{crit} \approx 7 \times 10^4$. This would correspond to the Re for a 10-cm chord in a 10-m/sec airflow at 20°C – in other words, in a regime of some importance to birds and bats. These complications translate directly to tremendous uncertainties in estimating the form drag of wings and bodies, or of D_{pro} and D_{par}, in the literature (Refs. 31, 32), where the drag coefficients $C_{D,par}$ and $C_{D,pro}$, measured for the bodies and wings of birds in wind tunnels appear to decrease across the critical Reynolds number range. The changes in wing profile and planform geometry with flight speed U in free flight further complicate matters.

7. Progress and open problems in theory and measurement

In the lower Reynolds number range of insect flight ($Re < 10^4$), quantitative measurements of airfoil properties are not common (Refs. 26, 28). The unsteady flow will likely be dominated by large-scale *laminar* separation bubbles, and little is yet known of the qualitative details (see Ref. 33 for an authoritative discussion, Ref. 34 for some low Re airfoil experiments, and Ref. 35 for a summary of some live wind-tunnel experiments). However, the lower Re time-dependent problem is becoming amenable to direct numerical simulation following dramatic improvements in computer hardware and software performance (and price, in the former case). Recently, for example, Gustafson and Leben (Ref. 36) applied a multigrid Navier-Stokes code to a plunging and pitching two-dimensional flat-plate configuration, as investigated experimentally by Freymuth (Ref. 37) and the strongly separated flow and vortex-wake signatures were reproduced with good qualitative agreement.

The full two- and three-dimensional Navier-Stokes equations have also been solved in discrete lattice-gas automata models, that have become increasingly sophisticated, and "correct," in the sense of preserving invariants and isotropies of the continuous Navier-Stokes equations (c.f. Refs. 38–42). Because they use simple local neighborhood update, or collision, rules, the cellular-automaton model lends itself very well to parallelization on SIMD machines (single instruction multiple data – where a single operation is performed simultaneously on a large number of parallel processors on data local to each processor). Special Navier-Stokes computers have even been developed (Refs. 43, 44), although they have yet to find routine use in even moderate Reynolds number fluid flow problems.

Nonetheless, the approach is an exciting one, well-suited for time-dependent problems with complex boundaries, and also well-positioned to capitalize on predicted progress in massively parallel computing.

The inclusion of a satisfactory turbulence model into current, more conventional DNS schemes will serve to extend their useful Re range (c.f. Peskin, this volume). Computational issues in viscous-inviscid modeling of unsteady airfoil flows have been reviewed by McCroskey (Refs. 45, 46), and a comprehensive summary of state-of-the-art computational methods in viscous aerodynamics can be found in Reference 47. Although higher Re flows remain out of reach of current DNS techniques, there has also been significant progress in vortex methods in unsteady separated flows (c.f. Refs. 48, 49 for early work, and Refs. 50, 51 for clear reviews). Computational efficiency and considerable analytical convenience arise from the consideration of pointwise concentrations (or clouds, or patches) of vorticity within an inviscid flow field. The further study of the vortex dynamics of complex wakes and bodies, and their interactions, promises to be productive, with clear potential for animal flight studies.

Returning to the original discussion of unsteady, inviscid analytical models, quantitative estimates of the magnitude of the unsteady and three-dimensional effects can be made for a large portion of the k range of interest in animal flight. Although these estimates do not include flow separation and other viscous effects, they still represent improvements over the steady-state assumption, and many of the models could be extended further.

Because k falls with increasing U, linear unsteady model approximations become more readily applicable. Nonetheless, D_{par} and D_{pro} constitute a larger fraction of the total drag, and uncertainties in their estimation can become major sources of error in performance estimates for the whole animal. There is much to be learned concerning the origin, prediction, and control of separation at $Re < 10^6$, even in steady flows. Indeed, one must include a caveat that it is by no means obvious how, or even whether, lessons from the steady-state separation problem will transfer to the *unsteady* case.

8. Conclusions

It has been argued that the classic steady/unsteady debate should be replaced by a more quantitative discussion concerning the likely *magnitude* of the unsteady effects, which can often at least be roughly estimated for a given k. Such a shift would simply reflect the increasing sophistication and power of the analytical techniques and computational resources that have become available since the genesis of the discussion in the 1950's. On the other hand, there are many outstanding problems that remain unvolved, many deriving ultimately from separation in viscous boundary layers and the appearance of fluid turbulence in the higher Reynolds number domains. Some of these problems constitute formidable, and by the same token, exciting challenges.

Acknowledgments

I would like to thank my colleague, Dr. H.K. Cheng, for his valuable and friendly advice and support, and also Kelly Khademi, for patient and careful assistance with the manuscript and figures.

References

1. Spedding, G.R.: The Aerodynamics of Flight. The Mechanics of Animal Locomotion, RMcN Alexander, ed., Adv. Comp. Physiol., Springer-Verlag, 1991.
2. Batchelor, G.K.: An Introduction to Fluid Dynamics. Cambridge University Press, 1967.
3. Weis-Fogh, T.; and Jensen, M.: Biology and Physics of Locust Flight. I. Basic Principles in Insect Flight. A critical Review. Phil. Trans. R. Soc. London B, vol. 239, 1956, pp. 415–458.
4. Weis-Fogh, T.: Biology and Physics of Locust Flight. II. Flight Performance of the Desert Locust (*Schistocerca gregaria.*) Phil. Trans. R. Soc. London B, vol. 239, 1956, pp. 459–510.
5. Jensen, M.: Biology and Physics of Locust Flight. III. The Aerodynamics of Locust Flight. Phil. Trans. R. Soc. London B, vol. 239, 1956, pp. 511–552.
6. Weis-Fogh, T.: Quick Estimates of Flight Fitness in Hovering Animals, Including Novel Mechanisms for Lift Production. J. Exp. Biol., vol. 59, 1973, pp. 169–230.
7. Pennycuick, C.J.: Mechanics of Flight. Avian Biology, Volume 5, D.S. Farmer and J.R. King eds., Academic Press, London, 1975, pp. 1–75.
8. Norberg, U.M.: Aerodynamics, Kinematics and Energetics of Horizontal Flapping Flight in the Long-Eared Bat; *Plecotus auritus.* J. Exp. Biol., vol. 65, 1976, pp. 179–212.
9. Dudley, R.; and Ellington, C.P.: Mechanics of Forward Flight in Bumblebees. II. Quasi-Steady Lift and Power Requirements. J. Exp. Biol., vol. 148, 1990, pp. 148–153.
10. Cloupeau, M.; Devillers, J.R.; and Devezeau, D.: Direct Measurements of Instantaneous Lift in Desert Locust; Comparison with Jensen's Experiments on Detached Wings. J. Exp. Biol., vol. 80, 1979, pp. 1–15.
11. Cheng, H.K.; and Murillo, L.E.: Lunate-Tail Swimming Propulsion As a Problem of Curved Lifting Line in Unsteady Flow. Pt. 1. Asymptotic Theory. J. Fluid Mech., vol. 143, 1984, pp. 327–350.
12. Chopra, M.G.: Large Amplitude Lunate-Tail Theory of Fish Locomotion. J. Fluid Mech., vol. 74, 1976, pp. 161–182.
13. Katz, J.; and Weihs, D.: Hydrodynamic Propulsion By Large-Amplitude Oscillation of an Airfoil with Chordwise Flexibility. J. Fluid Mech., vol. 88, 1978, pp. 485–497.
14. Karpouzian, G.; Spedding, G.R.; and Cheng, H.K.: Lunate-Tail Swimming Propulsion. Pt. 2. Performance Analysis. J. Fluid Mech., vol. 210, 1990, pp. 329–351.
15. Lighthill, M.J.: Aquatic Animal Propulsion of High Hydromechanical Effeciency. J. Fluid Mech., vol. 44, 1970, pp. 265–301.
16. Phlips, P.J.; East, R.A.; and Pratt, N.H.: An Unsteady Lifting-Line Theory of Flapping Wings with Application to the Forward Flight of Birds. J. Fluid Mech., vol. 112, 1981, pp. 97–125.
17. Azuma, A.; Azuma, S.; Watanabe, I.; and Furuta, T.: Flight Mechanics of a Dragonfly. J. Exp. Biol., vol. 116, 1985, pp. 79–107.
18. Azuma, A.; and Watanabe, T.: Flight Performance of a Dragonfly. J. Exp. Biol., vol. 137, 1988, pp. 221–252.
19. Gursal, I.; and Ho, C-M.: High Aerodynamic Loads on an Airfoil Submerged in an Unsteady Stream. AIAA Paper, 1991, in press.
20. Lighthill, M.J.: On the Weis-Fogh Mechanism of Lift Generation. J. Fluid Mech., vol. 60, 1973, pp. 1–17.
21. Maxworthy, T.: Experiments on the Weis-Fogh Mechanism of Lift Genereation by Insects in Hovering Flight. Pt. 1. Dynamics of the "Fling." J. Fluid Mech., vol. 93, 1979, pp. 47–63.
22. Edwards, R.H..; and Cheng, H.K.: The Separation Vortex in the Weis-Fogh Circulation-Generation Mechanism. J. Fluid Mech., vol. 120, 1982, pp. 63–473.

23. Spedding, G.R.; and Maxworthy, T.: The Generation of Circulation and Lift in a Rigid Two-Dimensional Fling. J. Fluid Mech., vol. 165, 1986, pp. 247–272.
24. Wu, J.; and Hu-Chen, H.: Unsteady Aerodynamics of Articulate Lifting Bodies. AIAA Paper 2184, 1984.
25. Haussling, H.J.: Boundary-Fitted Coordinates for Accurate Numerical Solution of Multibody Flow problems. J. Comp. Phys., vol. 30, 1979, pp. 107–124.
26. Lissaman, P.B.S.: Low-Reynolds-Number Airfoils. Ann. Rev. Fluid Mech., vol. 15, 1983, pp. 223–239.
27. Cheng, H.K.; and Smith, F.T.: The Influence of Airfoil Thickness and Reynolds Number on Separation. J. Appl. Math Phys. (ZAMP), vol. 33, 1982, pp. 151–180.
28. Schmitz, F.W.: Aerodynamik des Flugmodells. Karl Lange, Duisberg, 1960.
29. Jones, R.T.: Wing Theory. Princeton University Press, Princeton, N. J., 1990.
30. Lee, C.J.; and Cheng, H.K.: An Airfoil Theory of Bifurcating Laminar Separation from Thin Obstacles. J. Fluid Mech., vol. 216, 1990, pp. 255–284.
31. Pennycuick, C. J.; Obrecht, H.H.; and Fuller, M.R.: Empirical Estimates of Body Drag of Large Waterfowl and Raptors. J. Exp. Biol., vol. 135, 1988, pp. 253–264.
32. Tucker, V.A.: Body Drag, Feather Drag and Interference Drag of the Mounting Strut in a Peregrine Falcon, *Falco peregrinus*. J. Exp. Biol., vol. 149, 1990, pp. 449–468.
33. Ellington, C.P.: The Aerodynamics of Hovering Insect Flight. I. The Quasi-Steady Analysis. II. Morphological Parameters. III. Kinematics. IV. Aerodynamic Mechanisms. V. A. Vortex Theory. VI. Lift and Power Requirements. Phil. Trans. R. Soc. London, B, vol. 305, 1984, pp. 1–181.
34. Freymuth, P.: The Vortex Patterns of Dynamic Separation: A Parametric and Comparative Study. Prog. Aerospace Sci., vol. 22, 1985, pp. 161–208.
35. Luttges, M.W.: Accomplished Insect Fliers. Frontiers in Experimental Fluid Mechanics, M. Gad el Hak, ed., Springer-Verlag, Berlin, 1989, pp. 429–456.
36. Gustafson, K.; and Leben, R.: Computation of Dragonfly Aerodynamics. Comp. Phys. Comm., 1991, in press.
37. Freymuth, P.: Thrust Generation By an Airfoil in Hover Modes. Exp. Fluids, vol. 9, 1990, pp. 17–24.
38. Frisch, U.; Hasslacher, B.; and Pomeau, Y.: Lattice-Gas Automata for the Navier-Stokes Equation. Phys. Rev. Lett., vol. 56, 1986, pp. 1505–1508.
39. d'Humieres, D.; Lallemand, P.; and Frisch, U.: Lattice Gas Dynamics for 3*D* Hydrodynamics. Europhys. Lett., vol. 4, 1986, pp. 291–297.
40. Frisch, U.; d'Humieres, D.; Hasslacher, B.; Lallemand, P.; Pomeau, Y.; and Rivet, J.P.: Lattice Gas Hydrodynamics in Two and Three Dimensions. Complex Sys., vol. 1, 1987, pp. 649–707.
41. Fahner, G.: A Multispeed Model for Lattice-Gas Hydrodynamics. Complex Sys., vol. 5, 1991, pp. 1–14.
42. Wolf-Gladrow, D.A.; Nasilowski, R.; and Vogeler, A.: Numerical Simulations of Fluid Dynamics with a Pair Interaction Automaton in Two Dimensions. Complex Sys., vol. 5, 1991, pp. 89–100.
43. Clouqueur, A.; and d'Humieres, D.: RAP1, a Cellular Automata Machine for Fluid Dynamics. Complex. Sys., vol. 1, 1987, pp. 585–597.
44. Margolus, N.; and Toffoli, T.: Cellular Automata Machines. Complex Sys., vol. 1, 1987, pp. 967–993.
45. McCroskey, W.J.: The Phenomenon of Dynamic Stall. NASA TM 81264, 1981.
46. McCroskey, W.J.: Unsteady Airfoils. Ann. Rev. Fluid Mech., vol. 14, 1982, pp. 285–311.
47. Murthy, T.K.S.; and Brebbia, C.A., eds.: Computational Methods in Viscous Aerodynamics. Elsevier, Amsterdam, 1990.
48. Sarpkaya, T.: An Inviscid Model of Two-dimensional Vortex Shedding for Transient and Asymptotically Steady Separated Flow over an Inclined Plate. J. Fluid Mech., vol. 68, 1975, pp. 109–128.
49. Katz, J.: A Discrete Vortex Method for The Non-Steady Separated Flow over an Airfoil. J. Fluid Mech., vol. 102, 1981, pp. 315–328.

50. Saffman, P.G.; and Baker, G.R.: Vortex Interactions. Ann. Rev. Fluid Mech., vol. 11, 1979, pp. 95–122.
51. Leonard, A.: Vortex Methods for Flow Simulation. J. Comp. Phys., vol. 37, 1980, pp. 289–335.

Department of Aerospace Engineering, University of Southern California, Los Angeles, California.

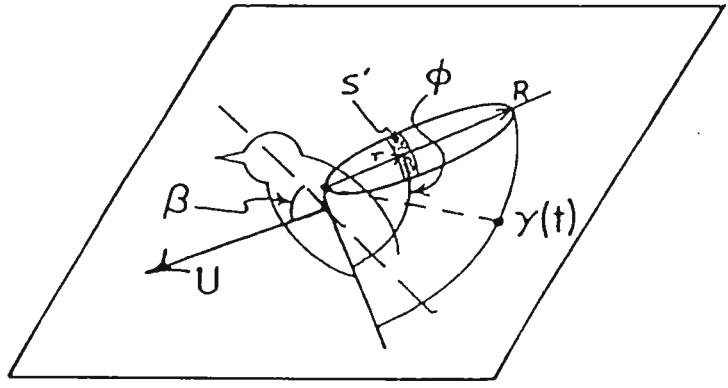

FIGURE 1. Notation for local section analysis of a flapping wing. The wing is divided into strips with area S' at distance r from the root. Given the local angle of attack, α, together with β, and ϕ, the local velocity $\vec{u}$ can be estimated at γ. This may, or may not, include local corrections for the induced downwash, w_i.

Reprinted with permission from "The aerodynamics of flight. The mechanics of animal locomotion" by G.R. Spedding, *Adv. Comp. Physiol.*, Vol. 11, pp. 51–111, Springer-Verlag, Figure 3.

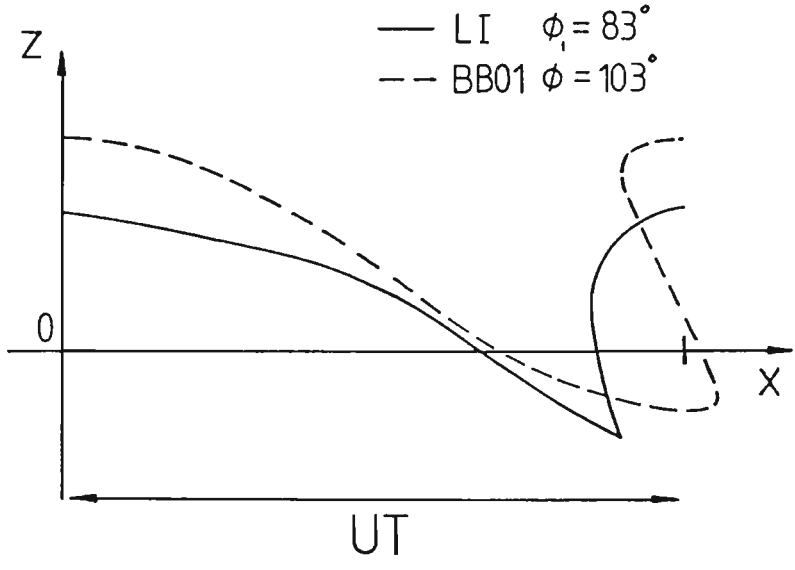

FIGURE 2. The traces of the wingtip through the air of the locust (from Fig. III4 (Ref. 5, solid curve)), and of the bumblebee in fast forward flight (from Fig. 16 in Ref. 16, dashed curve), rescaled by horizontal distance traveled during the stroke period. During this time, a section of locust forewing travels through about 15 chord lengths, while that of the bumblebee moves through about 6. Note that the wing-stroke amplitude ϕ of the bumblebee is higher than the locust's, and that the wings beat mostly above the horizontal plane at the wing root, $z = 0$. Consequently, the half-angle between the wings at the top of their cycle can be estimated to be only 23°, whereas it is 39° for the locust forewing. The locust hindwing trace is qualitatively similar but the stroke amplitude, $\phi_2 = 110°$.

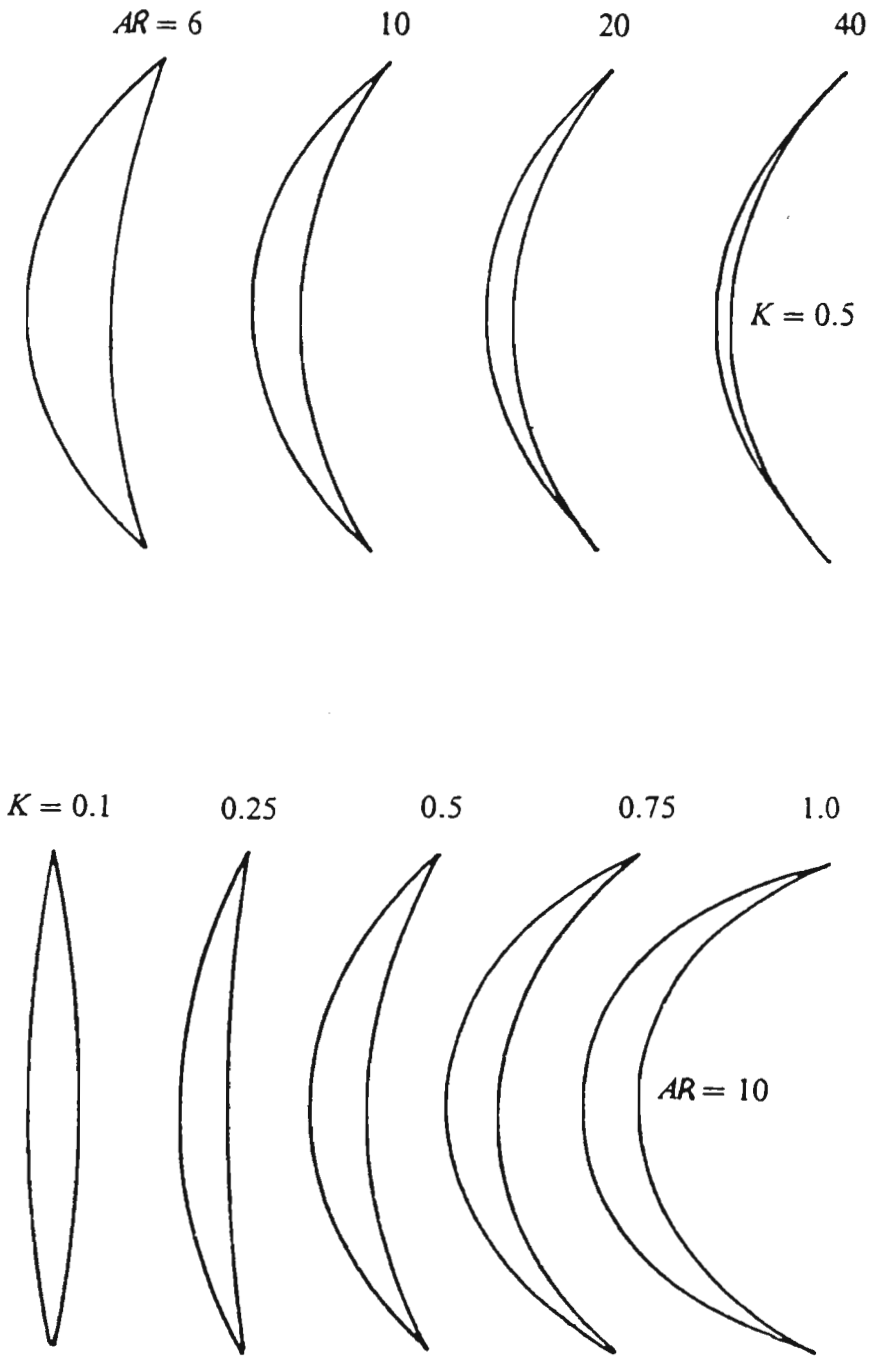

FIGURE 3. Two families of crescent-shaped lifting surfaces generated by varying the aspect ratio AR at a fixed sweep angle K, (top row), and by varying K for fixed $AR = 10$ (bottom row). The variations in K with $AR = 10$ correspond to the shapes discussed in Figures 4 and 5.

Reprinted from "Lunate-tail swimming propulsion. Part 2 performance analysis" by G. Karpouzian et al, *J. Fluid Mech.*, volume 210, 1990, pp. 329–351, Figure 5.

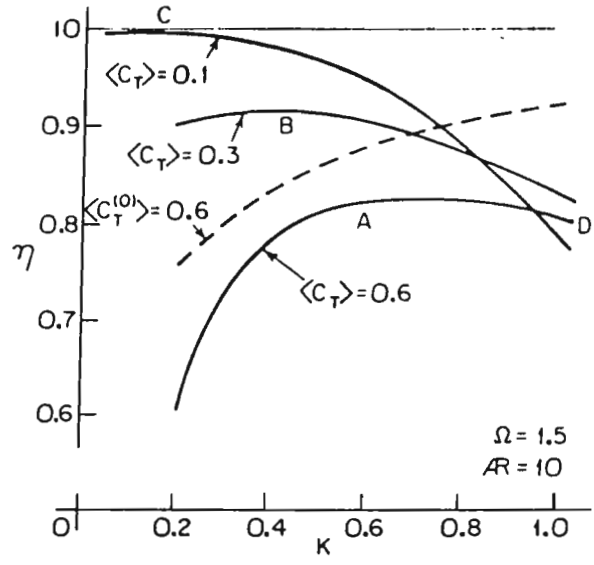

FIGURE 4. Propulsive efficiency η as a function of K, for three different values of $\langle C_T \rangle$, for the parabolic centerline (solid curves). The dashed line corresponds to the leading-order terms alone, equivalent to the two-dimensional, quasi-steady strip theory.

Reprinted from "Lunate-tail swimming propulsion. Part 2 performance analysis" by G. Karpouzian et al, *J. Fluid Mech.*, volume 210, 1990, pp. 329–351, Figure 6.

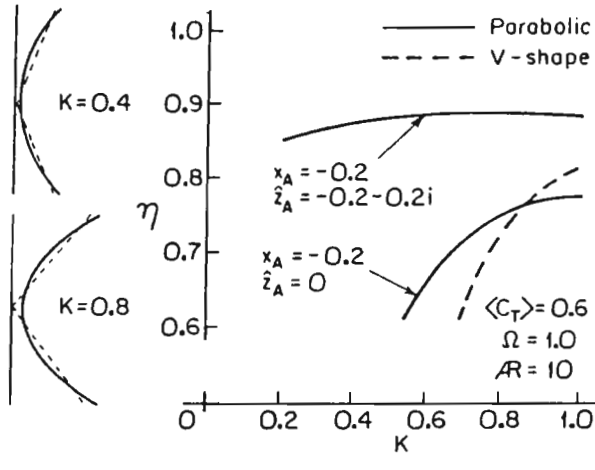

FIGURE 5. Performance of parabolic (solid curve) and V-shaped (dashed) centerlines. In the upper solid curve, $\hat{z}_A \neq 0$, corresponding to transverse displacements of the major pitch axis.

Reprinted from "Lunate-tail swimming propulsion. Part 2 performance analysis" by G. Karpouzian et al, *J. Fluid Mech.*, volume 210, 1990, pp. 329–351, Figure 10.

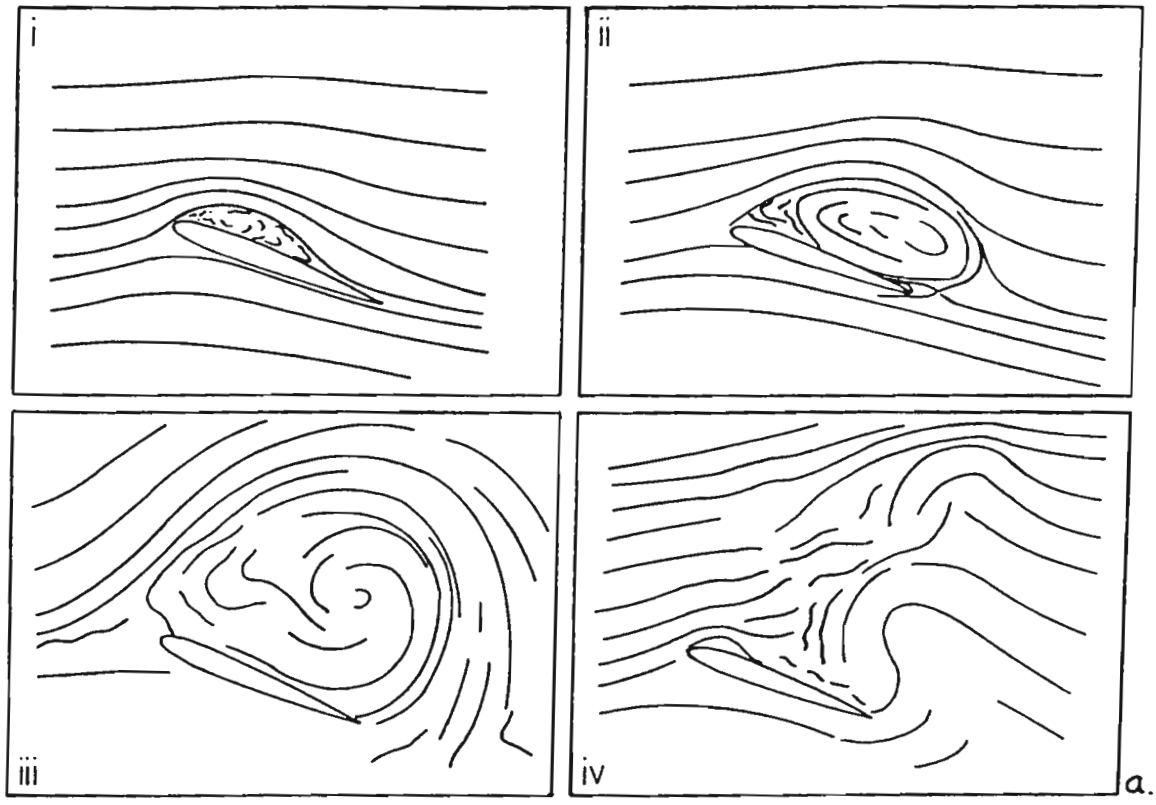

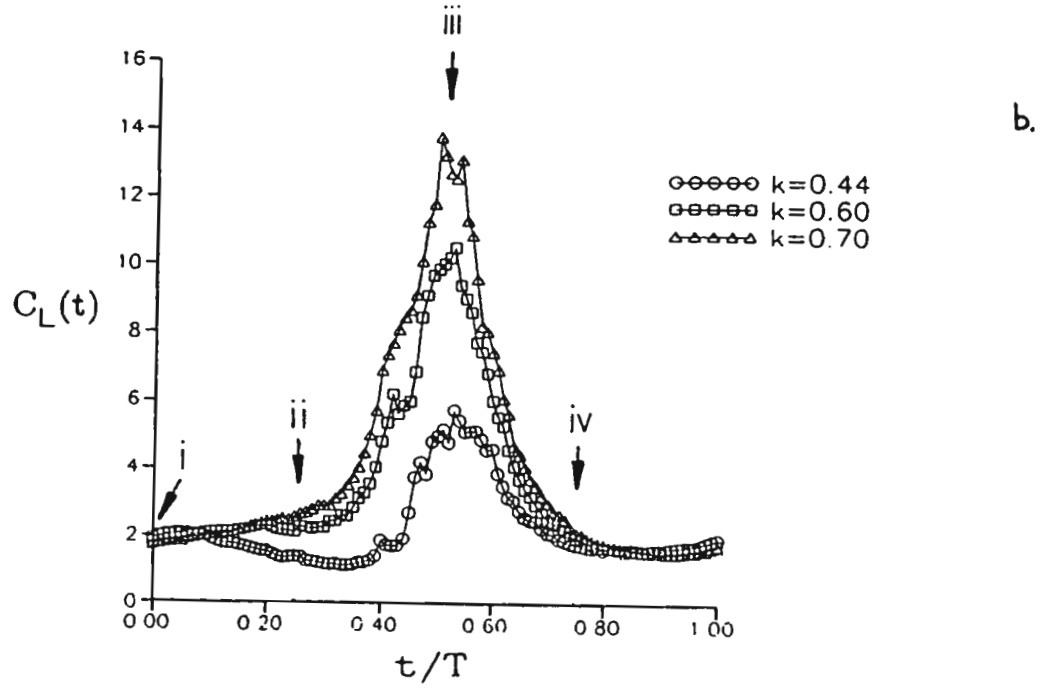

FIGURE 6. (a) Estimated instantaneous streamlines over a NACA 0012 airfoil investigated by Gursal and Ho (Ref. 19) at fixed $\alpha = 20°$ in an unsteady free stream ($k = 0.70$), drawn by tracing tangents to particle streak photographs supplied by the authors. (b) Phase-averaged instantaneous lift coefficients for different values of k.

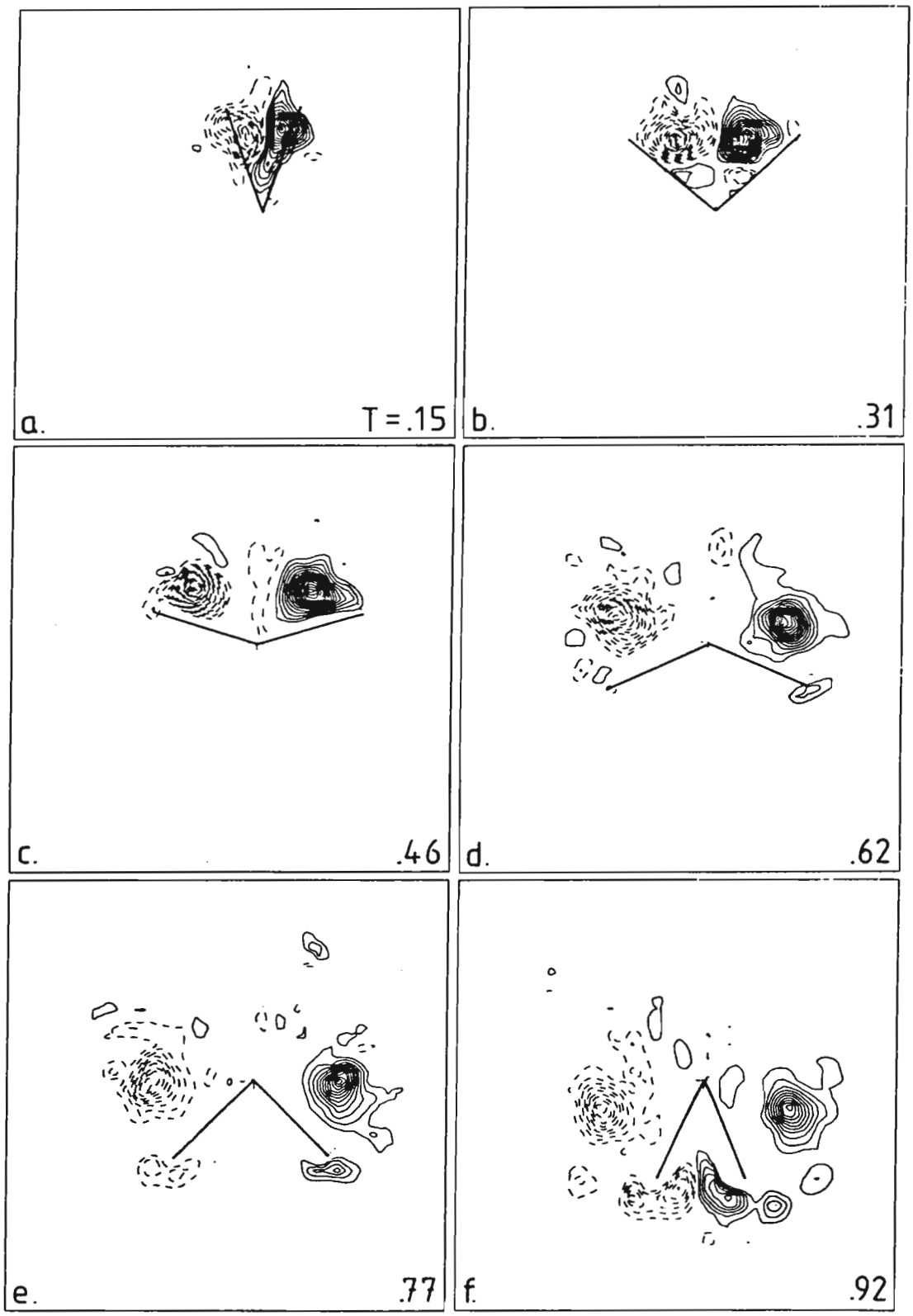

FIGURE 7. Contours of constant vorticity ω around a wing-pair opening by rotation along the common trailing edge. The contour interval is the same in all cases, corresponding to $\delta\omega = 0.025$/sec. The uncertainty in ω is approximately ± 1 contour level. The ω values were interpolated from irregularly spaced particle velocities onto a rectangular mesh by a two-dimensional patched, smoothing thin-shell spline. The flow very close to the wings cannot be resolved clearly.

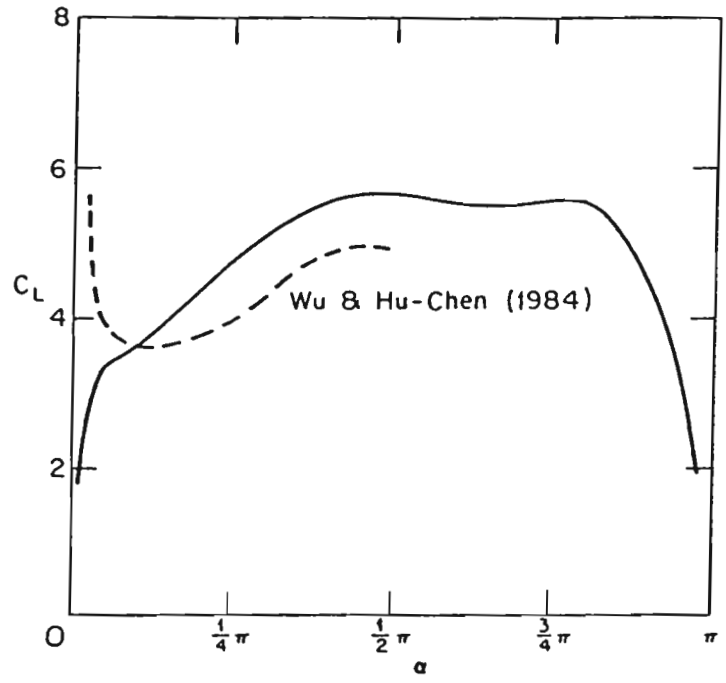

FIGURE 8. High instantaneous lift coefficients can be realized over much of the opening cycle. Agreement with a separation-vortex model (Ref. 24) is reasonable, and includes the plateau at $\alpha \approx 0.4\pi$.

Reprinted from "The generation of circulation and lift in a rigid two-dimensional fling" by G. R. Spedding and Maxworthy, *J. Fluid Mech.*, **165**, 247–272.

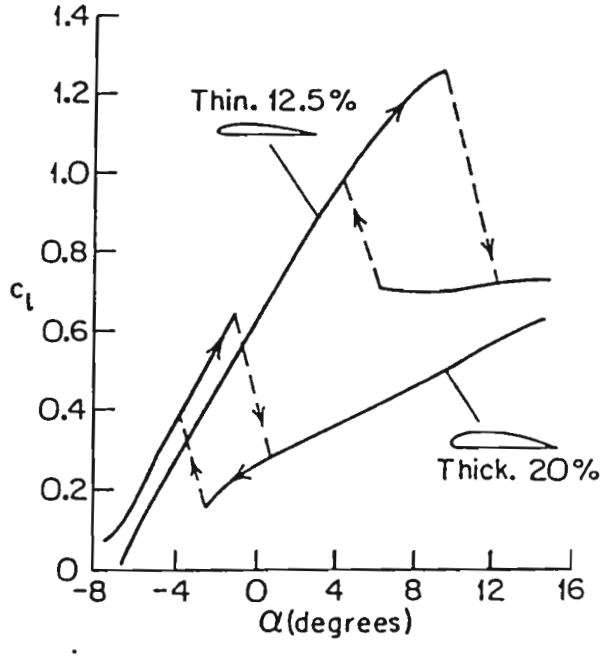

FIGURE 9. Lift hysteresis in airfoils of different thickness at $Re = 10^5$. From Reference 29 based on data in Reference 28.

Reprinted with permission from "The aerodynamics of flight. The mechanics of animal locomotion" by G.R. Spedding, *Adv. Comp. Physiol.*, Vol. 11, pp. 51–111, Springer-Verlag, Figure 8.